Drug Design, Development and Therapy

Dovepress
open access to scientific and medical research

Open Access Full Text Article

ORIGINAL RESEARCH

An Exosome-Based Therapeutic Strategy Targeting Neuroinflammation in Alzheimer's Disease with Berberine and Palmatine

Xin Zhao[1,*], Pingyuan Ge[1,*], Shaohua Lei[1], Siqi Guo[1], Peng Zhou[1], Li Zhao[1], Yiyu Qi[1], Xiaotong Wei[2], Weizhen Wu[2], Ningjing Wang[2], Rui Guo[3], Nianyun Yang[1], Qingqing Xiao[1], Qichun Zhang[1,2], Huaxu Zhu[1]

[1]Department of Traditional Chinese Medicine Processing and Preparation, Nanjing University of Chinese Medicine, Nanjing, Jiangsu, People's Republic of China; [2]Jiangsu Key Laboratory for Pharmacology and Safety Evaluation of Chinese Materia Medica, School of Pharmacy, Nanjing University of Chinese Medicine, Nanjing, People's Republic of China; [3]School of Medicine and Holistic Integrative Medicine, Nanjing University of Chinese Medicine, Nanjing, People's Republic of China

*These authors contributed equally to this work

Correspondence: Qichun Zhang; Huaxu Zhu, Email zhangqichun@njucm.edu.cn; zhuhx@njucm.edu.cn

Introduction: Neuroinflammation is one of the major pathogeneses in Alzheimer's disease (AD) and mainly involves abnormal inflammatory activation of microglia by multiple pathological stimuli. The treatment of AD remains a major challenge due to the multifactorial characterization of AD and the inefficient ability of therapeutic drugs to permeate through the blood–brain barrier (BBB). Accordingly, drug combination treatment and drug carrier delivery have become important therapeutic tools for the treatment of multifactorial diseases, especially AD.

Methods: Inflammatory cytokine levels in microglia, including NO, TNF-α, IL-1β, IL-4, and IL-10, were detected. The Morris water maze and object location task were used to investigate the learning and memory functions of APP/PS1 mice in different treatment groups. The number of neurons and plasticity of synapses were evaluated by immunofluorescence double labelling. Additionally, the ratio of β-amyloid plaques and the number of activated microglia were evaluated by immunofluorescence staining. The concentrations of β-amyloid plaques and inflammatory factors in the hippocampus were determined by ELISA. Microglia-derived exosomes (Exos) were extracted and purified by size exclusion chromatography. The distribution of exosomes and drugs was investigated in vitro and in vivo.

Results: Compared to single drug interventions, the combination of Ber and Pal (Ber/Pal) modulated microglial inflammatory cytokine levels. Ber/Pal promoted the recovery of learning and memory impairment in APP/PS1 mice. Immunofluorescence staining indicated that Ber/Pal restored neurons, inhibited Aβ plaque formation and microglial activation, and regulated the secretion of inflammatory factors. Exos promoted the accumulation of drugs in cells and tissues and improved the targeting of drugs across the BBB.

Conclusion: Ber/Pal could offer a synergistic and more comprehensive therapeutic effect in AD. Additionally, the microglia-derived Exos-Ber/Pal delivery system promoted the targeting and permeation of drugs into the brain, suggesting a creative strategy for targeting AD therapy by regulating neuroinflammation in microglial cells.

Keywords: Alzheimer's disease, neuroinflammation, phytoconstituents, drug combination, BBB permeability, exosomes

Introduction

Neuroinflammation, which has become the third major pathological feature in AD after β-amyloid (Aβ) deposition and neurofibrillary tangles, is an immune response activated by glial cells in the central nervous system (CNS), usually in response to stimuli such as nerve injury, Aβ plaques and tau neurofibrillary tangles or in response to autoimmunity. As the major inflammatory regulator in the CNS, microglia and their phenotypic modulation play a crucial role in regulating

Received: 18 April 2023
Accepted: 12 August 2023
Published: 17 August 2023

the progression of neurodegenerative diseases.[1] The phenotypic alternation of microglia mainly involves the M1 phenotype (proinflammatory) and the M2 phenotype (anti-inflammatory), and the release of inflammatory factors is an important physiological process for maintaining cerebral homeostasis.[2] Besides, a recent clinical epidemiological study revealed that the onset of neuroinflammation is associated with increased brain deposition of Aβ and tau, suggesting that the onset of neuroinflammation before the onset of cognitive symptoms may serve as an adaptive mechanism to prevent the accumulation of Aβ and tau proteins.[3] Accordingly, targeting neuroinflammation may provide a novel and promising therapy for AD.

Berberine (Ber) and palmatine (Pal) are isoquinoline alkaloids mainly isolated from *Rhizoma Coptidis* and have exhibited extensive pharmacological effects encompassing antioxidant, anti-inflammatory, antitumour, and neuroprotective effects.[4–6] In recent decades, the CNS efficacies of Ber and Pal have been widely investigated, and their therapeutic roles in neurological disorders, including Alzheimer's disease and Parkinson's disease, have been gradually explored and confirmed.[7,8] Additionally, considering the differences and similarities in chemical structure between Ber and Pal, they have different targets but exert similar pharmacological activities, possessing the feasibility and potential to treat diseases by means of combinational drug therapy.[9]

The blood–brain barrier (BBB) protects the brain from potentially harmful substances circulating in the bloodstream but also prevents most potential drugs from entering the CNS.[10] The need for new treatments for neurodegenerative diseases and the limitations imposed by the BBB are driving the adoption of nanotechnology.[11] Exosomes (Exos) are extracellular nanovesicles that participate in various physiological processes and exert pathological activities, including intracellular signalling and intercellular transport of protein and RNA.[12] Emerging clinicopathological and experimental studies have suggested the crucial role of Exos in intercellular communication and in the transportation of materials in the CNS and their excellent biocompatibility for drug delivery.[13] As a natural nanoscale delivery system directly secreted and isolated from various cell types, Exos inherit the components of parental cells and therefore have excellent biocompatibility to prevent clearance by the immune system and even the capability of passing through the BBB.[14] Besides, considering that specific surface molecules are expressed on the surface of exosomes during the formation and secretion process, Exos also exhibit the characteristic of specific cell natural targeting.

In this study, an APP/PS1 AD mouse model and an Aβ peptide-stimulated microglial cell model were used to explore the therapeutic role of Ber and Pal in AD. Additionally, to investigate the feasibility and therapeutic role of codelivery systems of Ber and Pal combined treatment in AD, we performed cellular and animal experiments. Eventually, to enhance BBB permeability through the blood–brain barrier and cellular drug targeting ability, microglia-derived Exos were adopted as carriers for the combined delivery of Ber and Pal, and the pharmacology and potential mechanisms were initially explored.

Materials and Methods

Materials and Reagents

Ber and Pal were purchased from Macklin (Chengdu, China). Sphingolipid mixed standards were purchased from Avanti Polar Lipids (USA). Size exclusion columns were provided by IZon Science (New Zealand). Latex beads were obtained from Sigma–Aldrich (St. Louis, MO, USA). A LIPID MAPS internal standard cocktail was purchased from Avanti Polar Lipids (Alabaster, USA). Aβ peptide (25–35) ($A\beta_{25\text{-}35}$) was obtained from Beijing Bosen Biotechnology Co., Ltd. (Beijing, China). The PKH26 fluorescent probe was purchased from Maokangbio (Shanghai, China). Enzyme-linked immunosorbent assay (ELISA) kits for TNF-α, IL-1β, IL-4, IL-10, $A\beta_{40}$, and $A\beta_{42}$ were obtained from Beijing Sinouk Institute of Biological Technology (Beijing, China). Anti-NeuN, anti-ionized calcium-binding adapter molecule 1 (IBA-1) and anti-postsynaptic density 95 (PSD95) were purchased from AiFanglogical (Hunan, China). A nitric oxide (NO) assay kit was obtained from Beyotime (Shanghai, China). DiR iodide and the Cell Counting Kit-8 (CCK-8) were purchased from MedChemExpress (New Jersey, USA). Microglia were purchased from the National Biomedical Cell-Line Resource Center (Beijing, China). Human neuroblastoma cells (SH-SY5Y) were purchased from the Institute of Biochemistry and Cell Biology (Shanghai, China).

Animals

SPF male APP/PS1 (B6; C3-Tg (APPswe, PSEN1dE9)) double transgenic mice (16 weeks), weighing 30 ± 3 g, were purchased from Jiangsu Huachuang Sino Pharma Tech Co., Ltd., and used as the AD model. SPF male B6C3 mice (16 weeks), weighing 30 ± 3 g, were used as controls (wild type, WT). The mice were adaptively reared for 8 weeks (24 weeks).

Culture of Microglial Cells and Extraction of Exos

Microglia were cultured in high-glucose DMEM with 10% FBS (VivaCell, Shanghai, China) and 1% penicillin–streptomycin solution at 37 °C and 5% CO_2 in a humidified atmosphere. When microglia reached 60–70% confluence, the culture medium containing 10% exosome-depleted FBS was used to continue the culture for 24 h, and the cell supernatant was collected. The collected supernatant was centrifuged at 300 × g for 5 min, 2000 × g for 10 min, and 10,000 × g for 30 min in turn at 4 °C. Afterwards, the cell supernatant was concentrated through ultrafiltration tubes (100 kD). Finally, the Exos were extracted and purified by size exclusion chromatography. The characterization methods of exosomes include transmission electron microscopy (TEM), nanoparticle tracking analysis (NTA) and Western blotting (WB). The morphology of Exos was observed by TEM (HT-7800, HITACHI, Japan). The particle size and potential were determined by NTA (NS300, Malvern, UK). The marker proteins of Exos, including CD63 and TSG101, were identified by WB.

Detection of Sphingolipid Metabolism

To induce the Aβ polymer, sterile distilled water was used to dissolve $A\beta_{25\text{-}35}$ at a concentration of 1 mM and incubated for 7 days at 37 °C. Microglia were treated with $A\beta_{25\text{-}35}$ (20 μM). Moreover, microglia were separately given Ber, Pal, jatrorrhizine (Jat), berberrubine (Brb), wogonin (Wog), baicalin (Bai), oroxylin A (OA), gardenin B (GB), and geniposide (Gen) for 24 h (all concentrations were 1 μM), and the supernatant was collected. The concentrations of sphingosine-1-phosphate (S1P) and ceramide (Cer) were determined by LC–MS (AB SCIEX Triple Quad^{TM}, AB SCIEX, USA). The specific experimental conditions of LC–MS have been previously reported.[15]

Detection of the NO Concentration

Microglia were stimulated with LPS (250 ng/mL) for 1 h and then incubated with Ber, Pal and a combination of Ber and Pal (Ber/Pal) for 24 h. The concentration of Ber/Pal was 0.3 μM. Moreover, microglia were stimulated with LPS for 1 h and then incubated with Ber/Pal, Exos, and Ber and Pal-coloaded Exos (Exos-Ber/Pal) for 24 h. The cell supernatant was collected to determine the concentration of NO.

Treatment of APP/PS1 Mice

Wild-type mice were used as the control group (WT). All AD mice were randomly divided into the model group (APP/PS1), Ber group (Ber), Pal group (Pal), Ber/Pal group (Ber/Pal), Exos group (Exos), and Exos-Ber/Pal group (Exos-Ber/Pal). Exos-Ber/Pal was administered at 1.22 mg/kg (Ber) and 1.5 mg/kg (Pal). The Exos group received the same amount of exosomes as the Exos-Ber/Pal (10 mg/kg). The Ber and Pal single drug groups were given the same amount of drugs as the Exos-Ber/Pal (1.22 mg/kg Ber; 1.5 mg/kg Pal). The mice were administered by tail vein injection at the same time every two days for a total of 21 days.

Morris Water Maze (MWM) Test

The mice were initially subjected to water maze training, and four trials were carried out from four different quadrants every day until most of the animals reached the platform quickly. Each trial lasted for 60s or until the animal found the platform. All animals were placed on the platform for 10s after each training session (including animals without the platform). The positioning navigation experiment lasted for 5 days. On the sixth day, the probe trial for 60s was performed, the platform was removed from the pool, and the time spent in the platform quadrant and the platform crossing time were measured.

Object Location Task (OLT)

During the training trial, the open field was placed with two distinct objects 6×6 cm away from their respective walls. Initially, experimental mice were gently placed in the fields facing the release corner and allowed to investigate the field and objects freely for 10 min. One of the two objects was replaced with a new location, and the animals were placed in the same way and allowed to freely investigate the field and objects freely for 10 min after 20 min of rest. Eventually, the investigation time of each mouse with each object was recorded and analysed.

ELISA

Inflammatory cytokines in the hippocampus tissues, including TNF-α, IL-1β, IL-4, and IL-10, were measured utilizing ELISA kits following the protocols from the instructions. Briefly, standard and tissue samples were added to each well and incubated for 1 h. Finally, the termination solution was utilized after adding the chromogenic agent for 15 min. OD values were measured at 450 nm using an enzyme-labelled instrument. The concentrations of $A\beta_{42}$ and $A\beta_{40}$ were determined by ELISA kits, and the protocol was the same as that used for inflammatory detection.

Immunofluorescence (IF) Staining

Fresh brain tissues were fixed in 4% paraformaldehyde (PFA) for 24 h. Subsequently, the samples were dehydrated with xylene and alcohol in each gradient (75–100%). The waxed tissue was embedded in a tissue embedder and cut to the micron level in a slicer. The sections were incubated with BSA. Then, micrometre-thick slices were incubated with different antibodies overnight. Appropriate secondary antibodies were used at RT for 50 min followed by incubation with DAPI. Fluorescence microscopy and a panoramic scanner were used to acquire images. ImageJ was used for analysis. The average fluorescence intensity of PKH26 and PSD95 was calculated. The Aβ staining area (%) was calculated relative to the total area of the analysed region (area% = plaque area/total area selected × 100%). The number of NeuN-positive cells was counted manually (cortex) and through software (hippocampus). In addition, the number of IBA-1-positive cells was counted by ImageJ.

Thioflavin S (Th-S) Staining

Th-S staining was performed after IF staining. Briefly, the sections were washed with PBS and stained in a 1% Th-S staining solution. Then, the sections were washed in 50% ethanol and PBS. The fluorescence images were detected by a fluorescence microscope after sealing.

BBB Permeability Prediction and Bioinformatics Analysis

The chemical structures of Ber and Pal were collected and downloaded from the ZINC database (https://zinc.docking.org/), and the structure files were imported into DeeP-red-BBB (https://github.com/12rajnish/DeePred-BBB) and LightBBB for drug combination and BBB permeability prediction. The potential targets of Ber and Pal were obtained from the SwissTargetPrediction online service (http://www.swisstargetprediction.ch/), and bioinformatics analysis was performed with the Metascape online database (https://metascape.org/gp/).

Analysis of the Phagocytic Capacity of Microglia

In the cell phagocytosis test, LPS-stimulated (250 ng/mL) microglia were incubated with Ber, Pal, and Ber/Pal for 24 h. Fluorescent latex beads (red) were coincubated with cells for 2 h. Microglia were washed with PBS and fixed with 4% PFA. Then, microglia were stained with DIO (green) and DAPI (blue). The cells were washed with PBS after each stain. Finally, anti-fluorescence quenching agent was added to the samples, and they were stored in the dark. The samples were observed under fluorescence microscopy.

Drug Loading and Release in vitro

Exos were mixed with Ber (1.5 mg/mL) and Pal (2 mg/mL), and the system was ultrasonicated for 30s in an ice bath and then suspended for 30s. The system was stopped for 2 min every 6 min and cycled three times. Finally, the system was

placed in a water bath at 37 °C for 1 h, which was used to restore the membrane integrity of the Exos. Finally, free Ber and Pal were removed by ultrafiltration centrifuge tubes (50 kd). To compare the incubation method and freeze–thaw cycle, the release characteristics of Exos-Ber/Pal (Ber, 0.122 mg/mL; Pal, 0.15 mg/mL) were investigated utilizing PBS (pH 7.4) as the release medium and a dialysis bag (10 kd). The sealed dialysis bag was immersed in 50 mL of release medium (37 °C, 100 RPM). Release medium was taken at a predetermined time point, and an equal amount of fresh release medium was added. Detection was carried out by HPLC (e2695, Waters, USA). A 10-μL aliquot of sample solution was injected into a ZORBAX SB-C18 column (4.6 × 250 mm, 5 μm) maintained at 24 °C, and the flow rate was 0.8 mL/min. The mobile phase consisted of solvent C (acetonitrile) and solvent D (phosphoric acid: triethylamine: H_2O = 0.1:0.05:100, v/v/v). The column was eluted with 30% C:70% D at 347 nm for 12 min.

Uptake of Exos in vitro

In the in vitro uptake experiment, PKH26-labelled Exos (10 μg/mL) were incubated with microglia (BV2) and human neuroblastoma cells (SH-SY5Y) for 3 h. The cells were washed with PBS and fixed with 4% PFA. Then, the cells were stained with DAPI (blue). The cells were washed with PBS after each stain. Finally, the anti-fluorescence quenching agent was added to the samples, and they were stored in the dark. The samples were observed under a fluorescence microscope. In addition, microglia were incubated with labelled Exos for 30 min, 1 h, and 3 h to observe the uptake of Exos by the cells at different timepoints. The experimental steps were the same as before.

Distribution of Exos in vivo

In the in vivo distribution experiment, Exos were labelled with PKH26 (red) and administered to mice by tail vein injection. Mice were perfused at 6 h and 24 h with normal saline and 4% PFA solution, respectively, and the brain tissues were stored in 4% PFA overnight. The samples were placed in 15% sucrose solution, dehydrated at 4 °C, transferred to 30% sucrose solution and dehydrated at 4 °C. The samples were segmented after OCT embedding. Finally, the sections were stained with DAPI before full scanning. Additionally, DiR-labelled Exos (200 μg/mL) were administered to mice by tail vein injection. After administration, the mice were observed at 1, 3, 6, 9, 12 and 24 h by a live imaging instrument (IVIS Spectrum, PerkinElmer, USA).

Uptake of Ber and Pal in vitro

Exos-Ber/Pal and free Ber/Pal at the same concentration were added to microglia, and the cell supernatant was collected at 2, 4, 6, 12, and 24 h. After centrifugation of the collected cell supernatant, methanol: acetonitrile (1:3) was added to remove the protein. Finally, the samples were evaporated and redissolved in water (containing 0.1% formic acid). After filtration, the concentrations of Ber and Pal were determined by LC–MS. Chromatographic experiments were performed on a Vanquish UHPLC system (Thermo Scientific, USA). A 5-μL aliquot of sample solution was injected into an InfinityLab Poroshell 120 EC-C18 column (2.1 mm × 100 mm, 2.7 μm) maintained at 35 °C, and the flow rate was 0.3 mL/min. The mobile phase consisted of solvent A (formic acid: H_2O = 0.1:100, v/v/v) and solvent B (acetonitrile). The column was eluted with a gradient of 5 to 20% B at 0–1 min; 20% to 100% B at 1–5 min; 100% B at 5–5.5 min; 100% to 5% B at 5.5–6 min; and 5% B at 6–8 min. Mass spectrometry was performed on a TSQ Quantis system (Thermo Scientific, USA). The high energy spark-induced breakdown ionization (HESI) source adopted the positive ion scanning mode. The conditions used for the HESI source were as follows: ion spray voltage of 5500 V, ionization temperature of 550 °C, nebulizer gas pressure of 379.22 kPa, drying gas pressure of 379.22 kPa, and curtain gas pressure of 241.32 kPa.

Distribution of Ber and Pal in vivo

The mice were given Exos-Ber/Pal and free Ber/Pal at the same concentration by tail vein injection. After 24 h of administration, the brain (cortex, hippocampus, and striatum), heart, liver, spleen, and kidney were collected. After tissue homogenization, methanol: acetonitrile (1:3) was added to remove the protein. Finally, the samples were evaporated and redissolved in water (containing 0.1% formic acid). After filtration, the concentrations of Ber and Pal were determined by LC–MS. The conditions were the same as described above.

CCK-8 Test

Microglia were incubated with Ber/Pal (0.3 μM) and Exos for 24 h. Cell viability was measured utilizing CCK-8 kits following the manufacturer's instructions.

Statistical Analysis

All data are expressed as the mean ± standard deviation (SD). GraphPad Prism 8.0 was used to perform statistical analysis. Student's *t*-test was performed to compare the differences between groups. All other data were analysed using one-way ANOVA with Tukey's multiple comparisons test and Dunnett's multiple comparisons test. Statistical significance was assumed at $p < 0.05$. $p < 0.05$ is represented by "*", and $p < 0.01$ is represented by "**".

Results

Anti-Inflammatory Function of HLJDD Components in vitro

Drawing on our previous studies, Huanglian Jiedu decoction (HLJDD) could effectively rescue abnormal sphingolipid metabolism in AD model mice, especially S1P and Cer metabolism, which are critical potential hallmarks reflecting AD pathology. Accordingly, we screened the effective components in HLJDD based on the assessment criteria with the ratio of S1P/Cer in $A\beta_{25\text{-}35}$-stimulated microglia, and the cell supernatant was collected for LC–MS quantification. The LC–MS results showed that Ber and Pal significantly reversed the trend of S1P and Cer in $A\beta_{25\text{-}35}$-stimulated microglia (Figure S1A and B). Specifically, Ber and Pal markedly increased the S1P/Cer ratio (Figure S1C), and accordingly, Ber and Pal were selected for further exploration of AD therapeutic effects. To further verify the therapeutic effect of Ber/Pal on inflammation, we used LPS to stimulate microglial cells to become proinflammatory cells and then incubated them with Ber, Pal, and the combination of Ber and Pal (Ber/Pal). The NO measurement results showed that compared with a single drug, Ber/Pal more significantly inhibited the concentration of NO (Figure S2A). Additionally, we used latex beads to detect phagocytosis of microglia stimulated by LPS. The samples were observed under a fluorescence microscope (Figure S2B). The statistical results suggested that Ber/Pal more effectively inhibited the increase in phagocytosis caused by LPS stimulation than the single component (Figure S2C and D). Besides, to further verify the therapeutic effects of Ber, Pal and the combined therapy (Ber/Pal) on neuroinflammation in AD, LPS (250 ng/mL) and $A\beta_{25\text{-}35}$ (20 μM) were utilized to stimulate microglia for NO and inflammatory cytokine detection (Figure 1A–E). The results showed that Ber and Pal significantly reduced the release of NO and reversed the abnormal inflammatory cytokine levels in microglia stimulated by LPS and $A\beta_{25\text{-}35}$. Additionally, to evaluate the feasibility and therapeutic role of codelivery systems of Ber and Pal combined treatment in AD, a Ber and Pal combined treatment group was also included. Intriguingly, Ber/Pal exhibited more significant therapeutic effects on both NO and inflammatory cytokine release compared with the Ber and Pal single treatment groups.

Improvement in Cognitive Impairment and Nerve Injury in APP/PS1 Mice

To further investigate the therapeutic effects of Ber, Pal and Ber/Pal in vivo, we treated APP/PS1 mice with Ber, Pal and Ber/Pal by tail vein injection, and the experimental procedure is displayed in Figure 1F. After 14 days of treatment, behavioural tests, including the MWM and OLT, were performed to evaluate cognitive function in mice. The MWM is the most commonly used method for assessing spatial learning and memory function, which is closely associated with hippocampal synaptic plasticity and hippocampal activity.[16] As shown in Figure 1G–J, compared with the model group, the behavioural performance regarding the escape latency time in the positioning navigation experiment, platform crossing times and target quadrant occupancy in the probe trials were not significantly improved in the Ber, Pal and combined treatment groups. The OLT exploits the natural tendency of mice to interact with novel objects to reveal learning and memory, which rely on hippocampal activity.[17] Notably, the Ber/Pal combined treatment group exhibited significant optimal therapeutic effects in OLT experiment results (Figure 1K). Additionally, in the behavioural experiment, there were no significant differences in the average velocity and total activity among the different treatment groups, indicating that the movement of mice did not change due to strain and drug intervention (Figure S3). Cognitive dysfunction is normally initiated by neuronal damage and synaptic dysfunction. For further verification of whether

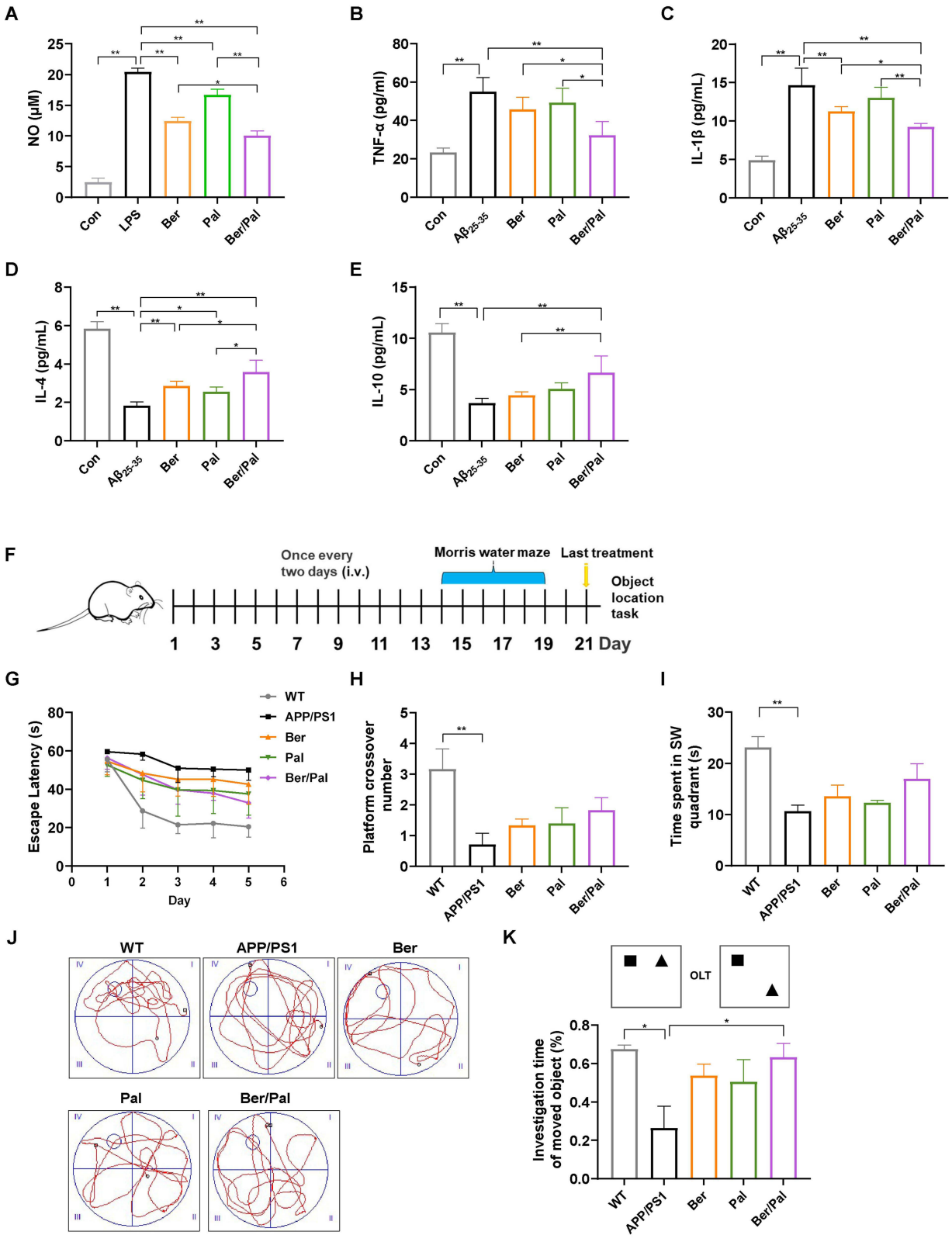

Figure 1 Effect of Ber, Pal and Ber/Pal combined treatment on neuroinflammation in vitro and behaviour in APP/PS1 mice. (**A**) The NO concentration in LPS-stimulated (250 ng/mL) microglia was detected with the Griess method. (**B**–**E**) Inflammatory cytokine detection of TNF-α, IL-1β, IL-4 and IL-10. Inflammatory cytokines in microglia stimulated by $A\beta_{25\text{-}35}$ (20 μM) after coincubation with Ber, Pal, Ber/Pal, Exos and Exos-Ber/Pal for 24 h. The microglia were stimulated with LPS/$A\beta_{25\text{-}35}$ for 1 h in advance. The concentration of Ber/Pal was 0.3 μM. (**F**) Schematic illustration of the experiment. (**G**) The escape latency time, (**H**) platform crossing times, and (**I**) target quadrant occupancy in the MWM. (**J**) Representative motion trajectories in the MWM. i, the first quadrant of MWM; ii, the second quadrant of MWM; iii, the third quadrants of MWM; iv, the fourth quadrants of MWM. (**K**) OLT performance of mice administered different formulations. WT indicates wild-type control mice without any gene intervention. APP/PS1 indicates the AD model mice. The Ber/Pal injection dosage was 1.22/1.52 mg/kg. (**A**), n = 3; (**B**–**E**), n = 6. (**F**–**K**), n = 8. *p < 0.05, **p < 0.01.

https://doi.org/10.2147/DDDT.S417465 DovePress

Ber, Pal and Ber/Pal could exert a neuroprotective effect on APP/PS1 mice, dual IF staining of NeuN and PSD95, which are important specific markers of neurons and synapses, was conducted in the different treatment groups. Compared with the AD model group, APP/PS1 mice treated with Ber or Pal displayed a higher number of NeuN-positive cells in the cortex and hippocampus (Figure 2A–C), indicating that neuronal survival was ameliorated by Ber and Pal treatment. Similar to the above results, the Ber/Pal combined treatment group exhibited more significant improvement in NeuN-positive cells in both the cortex and hippocampus than the Ber or Pal single treatment group. These results indicated that Ber, Pal and Ber/Pal rescued cognitive impairment and promoted the regeneration of neurons. However, there was no significant increase in PSD95 between the treatment groups and the model group (Figure 2D–G).

Inhibition of Aβ Pathology and Neuroinflammation in APP/PS1 Mice

Considering that the accumulation of Aβ peptides, plaques, microglia activation and neuroinflammation are notorious pathogenic characteristics of AD, dual staining of IBA-1 and Th-S was conducted to label microglia and identify Aβ plaques. Compared with the AD model group, IBA-1-labelled positive microglia and Th-S-labelled Aβ plaques were significantly decreased in the Ber, Pal and Ber/Pal groups, indicating ameliorated amyloidosis symptoms manifested by suppressed inflammatory microglial activation and attenuated neuroinflammation in APP/PS1 mice (Figure 3A–D). Besides, to further explore the potential mechanism of Ber, Pal and Ber/Pal on Aβ pathology and neuroinflammation, ELISA was utilized to measure the levels of cerebral $A\beta_{42}$, $A\beta_{40}$ and inflammatory cytokines. In comparison with the model group, treatment with Ber, Pal and Ber/Pal significantly reduced the levels of $A\beta_{42}$, $A\beta_{40}$, TNF-α, and IL-1β and increased the levels of IL-4 and IL-10 (Figure 3E–K). The overall results suggested the therapeutic effects of Ber, Pal and Ber/Pal combined therapy. Nevertheless, when these three groups were compared in parallel, we found that there were differences in the therapeutic effects of Ber and Pal, and the co-administered group always showed better and more comprehensive therapeutic effects, suggesting that the combination of Ber and Pal is a feasible approach for the treatment of AD. However, compared with the traditional cases of drug combination, there was relatively limited improvement in the therapeutic effects of Ber/Pal combined treatment. To probe into the underlying reason, BBB permeation prediction and target prediction were performed. The BBB permeation prediction results suggested poor BBB permeability of Ber and Pal (less than 30%), which is the reason for the relatively poor efficacy enhancement of the combination of Ber and Pal (Figure S4A–B). Additionally, the targets prediction results suggested that Ber and Pal had 45 common targets and a total of 111 differential targets, and the 111 different targets were enriched in inflammatory pathways and sphingolipid metabolism (Figures S4C–E and S5).

Exos-Ber/Pal Characterization

To enhance the BBB permeation and targeting ability of Ber/Pal combined treatment, microglia-derived Exos were prepared and utilized for drug delivery. Initially, to prepare the Exo-loaded Ber/Pal coloaded system (Exos-Ber/Pal), ultrasonication, incubation and freeze–thaw cycle methods were performed and assessed. Owing to the highest loading efficiency, the ultrasonication method was selected for drug delivery system preparation (Table 1). Subsequently, we performed particle size detection for characterization of Exos-Ber/Pal, and the particle size varied from 120 ± 2.6 nm (purified Exos) to 180.4 ± 11.7 nm (Exos-Ber/Pal) after drug loading, while the sphere morphology and characteristic proteins of Exos were preserved (Figure 4A–E), indicating that Exos-Ber/Pal was successfully prepared with a loading efficiency of 12.2% Ber and 15.2% Pal. Eventually, the release study showed that Ber and Pal were simultaneously released from Exos-Ber/Pal, and the cumulative release rates reached 72.59 ± 7.46% and 72.88 ± 9.90% at 48 h, respectively (Figure 4F). These data demonstrated that Exos-Ber/Pal could load Ber/Pal and possessed the biological and physical characteristics of Exos.

Exosomes Increased the Uptake of Free Drugs (Ber/Pal) in vitro and in vivo

To verify the cell-targeting ability of the Exos-Ber/Pal delivery system, we performed cellular uptake experiments in BV2 cell and SH cell models. As expected, an obvious fluorescent signal was observed in BV2 cells compared with SH cells after incubation with PKH26-labelled Exos for 3 h (Figure 5A). The quantitative data were consistent with the microscope images (Figure 5C), indicating that the isolated Exos could orient and target their parental cells. In addition, the cellular uptake of Exos-Ber/Pal showed a time-dependent nature, as shown in Figure 5B and D. The red fluorescent signal was improved, and the mean PKH26 fluorescent density increased with prolonged incubation time. Subsequently,

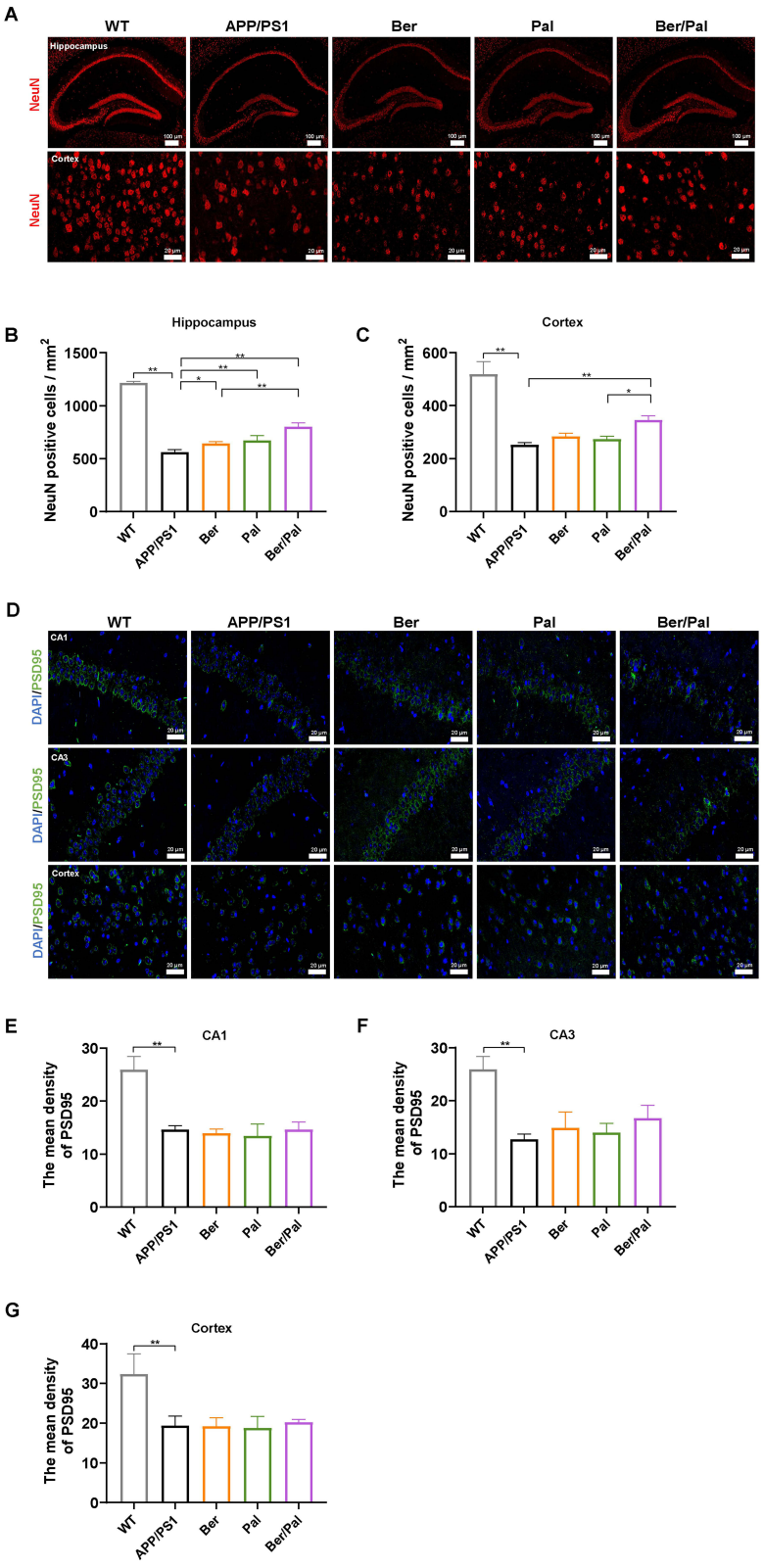

Figure 2 Effect of Ber, Pal and Ber/Pal combined treatment on neuronal recovery in APP/PS1 mice. (**A**) Immunofluorescence staining of NeuN-positive cells and (**B** and **C**) NeuN-positive cell counting in the hippocampus and cortex. (**D**) Immunofluorescence observation and (**E**–**G**) semiquantitative data of PSD95 in the CA1, CA3 and cortex. WT indicates wild-type control mice without any gene intervention. APP/PS1 indicates the AD model mice. The Ber/Pal injection dosage was 1.22/1.52 mg/kg. The scale bar for (**A**) is 100 μm (hippocampus) and 20 μm (cortex). The scale bar for (**D**) is 20 μm. n = 3. *p < 0.05, **p < 0.01.

https://doi.org/10.2147/DDDT.S417465 DovePress

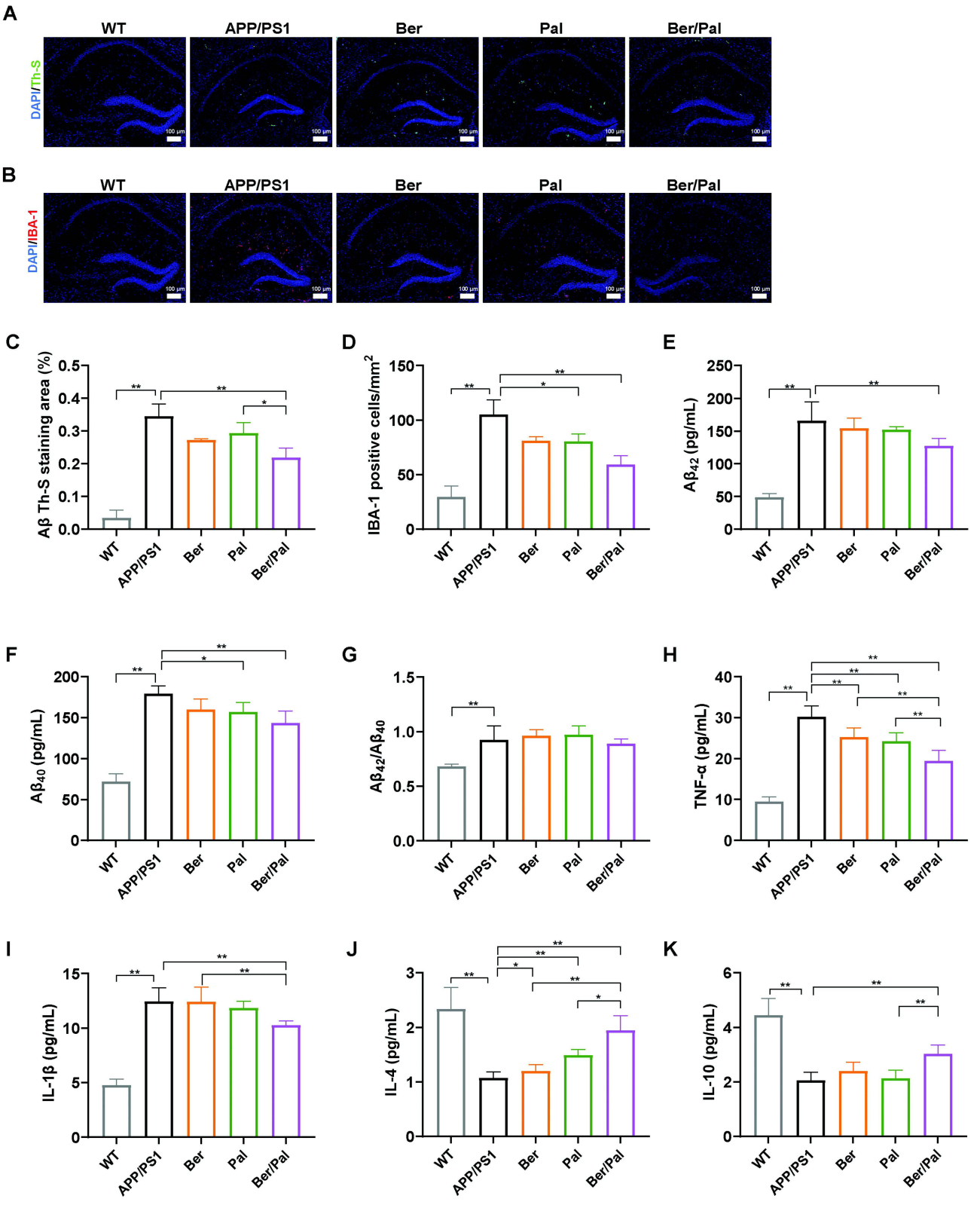

Figure 3 Inhibition of Aβ pathology and neuroinflammation in APP/PS1 mice. Immunofluorescence staining observation of (**A**) Th-S (Aβ) and (**B**) IBA-1 in the hippocampus. Quantitative analysis of (**C**) Aβ and (**D**) IBA-1. (**E**–**G**) Concentration determination of $A\beta_{42}$ and $A\beta_{40}$ and the ratio of $A\beta_{42}/A\beta_{40}$ in the hippocampus by ELISA. (**H**–**K**) Inflammatory cytokine detection in the hippocampus. WT indicates wild-type control mice without any gene intervention. APP/PS1 indicates the AD model mice. The Ber/Pal injection dosage was 1.22/1.52 mg/kg. The scale bar is 100 μm. (**A**–**D**), n = 3. (**E**–**K**), n = 5. *p < 0.05, **p < 0.01.

Table 1 Loading Efficiency of Incubation, Freeze-Thaw Cycles and Ultrasound

Method	Loading Efficiency (%)	
	Ber	Pal
Incubation	2.54±0.67	2.52±0.44
Freeze-thaw cycle	6.43±1.62	7.36±1.95
Ultrasonic	15.43±2.19	14.05±2.90

the cellular uptake of Exos-Ber/Pal was quantitated by determining the concentration of Ber/Pal by LC–MS. Compared with the Ber/Pal physical mixture, Exos-Ber/Pal showed a higher drug concentration in cells at the same time (Figure 5E and F), demonstrating that Exos enhanced cell phagocytosis and reduced cell clearance of the drug.

Positive targeting and drug accumulation in lesion sites have the potential to improve efficacy. Accordingly, to verify the distribution of Exos-Ber/Pal in vivo after circulation, we injected PKH26-labelled Exos into mice by the tail vein, and brains were collected at 6 h and 24 h. As shown in Figure 5G–J, an obvious red fluorescent signal was observed in the hippocampus and cortex, and the semiquantitative data were consistent with the qualitative pictures. Additionally, drug accumulation in the hippocampus, cortex, and striatum was detected by LC–MS after intravenous injection with the Ber/Pal physical mixture and Exos-Ber/Pal for 24 h. Our results suggested that the Exos carrier could prominently facilitate Ber and Pal entry into the brain, as the drug concentration in the physical mixture groups was significantly less than that in the Exos-Ber/Pal group (Figure 5K–L). The live imaging results further showed that Exos accumulated in the brain within 24 h (Figure S6). However, Ber and Pal were also measured in other tissues, especially in the heart and kidney (Figure S7). We hypothesized that systemic circulation of the particles led to their interaction with endogenous components and metabolism of the drug. Collectively, Exos-Ber/Pal could promote the targeting and permeation of drugs into the brain.

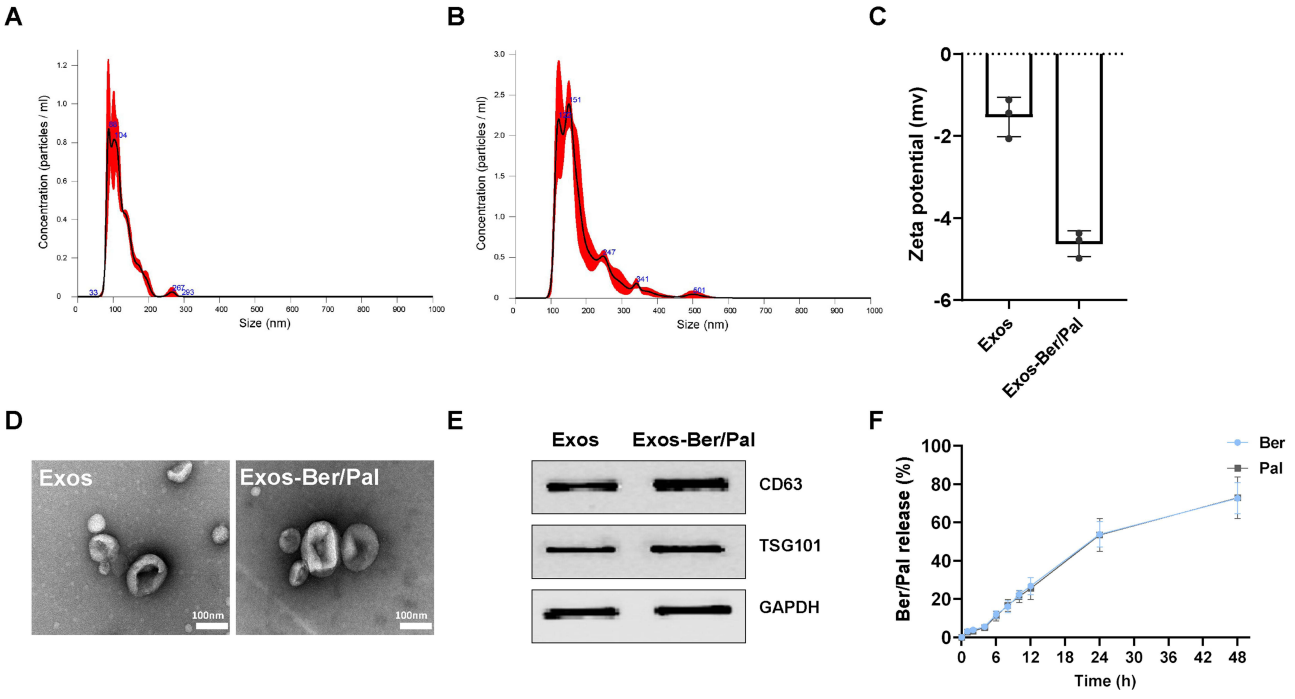

Figure 4 Characterization of Exos and Exos-Ber/Pal. (**A** and **B**) The particle size distribution of Exos and Exos-Ber/Pal. (**C**) Zeta potential. (**D**) TEM determination. (**E**) WB analysis of protein markers (CD63 and TSG101) in Exos and Exos-Ber/Pal. (**F**) Cumulative drug release from Exos-Ber/Pal in 48 h. The scale bar is 100 nm. n = 3.

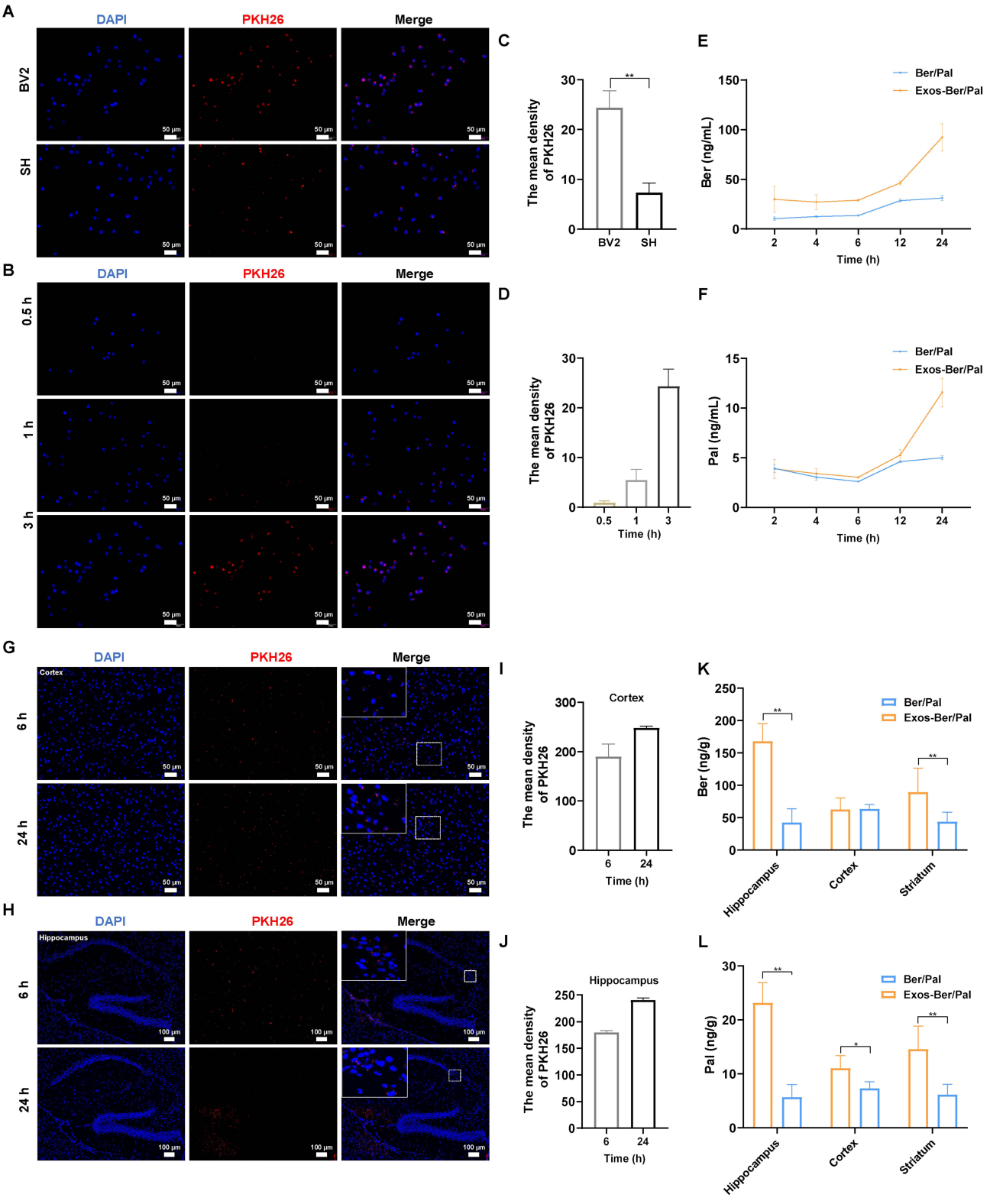

Figure 5 Distribution and targeting of Exos-Ber/Pal in vitro and vivo. (**A**) Parent cell targeting ability. Fluorescence images were observed by optimal microscopy. PKH26-labelled Exos were respectively incubated with BV2 and SH cells for 3 h. (**B**) Cellular uptake of PKH26-labelled Exos after incubation with BV2 cells for 0.5, 1 h and 3 h. (**C** and **D**) quantitative analysis of (**A** and **B**). (**E** and **F**) Uptake of Ber and Pal by microglia at 2, 4, 6, 12 and 24 h. The concentration of Ber/Pal was 0.3 μM. (**G** and **H**) Fluorescence imaging of cortex and hippocampus. PKH26-labelled Exos were intravenously injected for 6 h and 24 h. (**I** and **J**) quantitative data of (**G** and **H**). (**K** and **L**) Ber and Pal concentrations in the hippocampus, cortex and striatum were detected by LC-MS after intravenous injection with Ber/Pal and Exos-Ber/Pal for 24 h. The PKH26 was 2 μM. The Ber/Pal dosage was 0.88/1.13 mg/kg. The scale bar for (**A** and **B**) and (**G**) is 50 μm. The scale bar for (**H**) is 100 μm. (**A**–**J**), n = 3; (**K** and **L**), n = 6. *p < 0.05, **p < 0.01.

Exos-Ber/Pal Significantly Enhanced the Efficacy of Ber/Pal Free Drug Combination Treatment in vitro

Eventually, NO and inflammatory factors were measured using ELISA kits to evaluate the regulation of inflammation in LPS (250 ng/mL)- and $A\beta_{25-35}$ (20 μM)-stimulated microglia in vitro. As expected, and as the quantification results displayed, in comparison with LPS (250 ng/mL) and $A\beta_{25-35}$ (20 μM) stimulation in the Ber/Pal group, Exos-Ber/Pal treatment significantly reduced the production of NO, TNF-α and IL-1β and upregulated IL-4 and IL-10 expression (Figure 6A–E). Collectively, these results suggested that the microglia-derived Exos delivery method could enhance the therapeutic effects of Ber/Pal free drug treatment in vitro. In addition, the CCK-8 results showed that Ber/Pal and Exos did not affect cell viability (Figure S8).

Exos-Ber/Pal Significantly Enhanced the Efficacy of Ber/Pal Free Drug Combination Treatment in vivo

To verify the better therapeutic effects of Exos-Ber/Pal treatment, APP/PS1 mice were utilized to perform AD-associated behavioural and pathological indicator detection. The experimental procedure is displayed in Figure 6F. The behavioural results showed that, compared with the Ber/Pal free drug combination treatment (Ber/Pal) group, Exos-Ber/Pal treatment significantly reduced the escape latency time and increased the platform crossing times in the MWM (Figure 6G–H). Additionally, the time spent in the SW quadrant (Figure 6I–J) and the investigation time of the moved object in the OLT test (Figure 6K) were also prominently increased. Besides, NeuN and PSD95 were measured utilizing immunofluorescence staining to assess the therapeutic efficacy of Exos-Ber/Pal. The number of NeuN-positive cells in both the cortex and hippocampus and the fluorescence intensity of PSD95 in the hippocampus and cortex were significantly elevated compared with those in the Ber/Pal free drug combination treatment (Ber/Pal) group and the AD model group (Figure 7). These results suggested that Exos-Ber/Pal treatment could significantly augment the cognitive enhancement and neuroprotective efficacy of Ber/Pal free drug combination treatment.

Exos-Ber/Pal Could Enhance the Efficacy of Ameliorating Aβ Pathology and Neuroinflammation

Subsequently, to assess the therapeutic effects of ameliorating Aβ pathology and neuroinflammation after Exos-Ber/Pal treatment, IBA-1, Th-S, $A\beta_{40}$, $A\beta_{42}$, and inflammatory factors, including TNF-α, IL-1β, IL-4 and IL-10, were measured utilizing immunofluorescence staining and ELISA kits. In comparison with Ber/Pal-free drug treatment and the model group, Exos-Ber/Pal treatment significantly reduced microglial activation and the number of plaques in AD model mice (Figure 8A–D). Additionally, the $A\beta_{40}$ and $A\beta_{42}$ levels were also significantly reduced in the Exos-Ber/Pal treatment group compared with the AD model group and the Ber/Pal free drug treatment group (Figure 8E–G). Considering that microglial activation and Aβ pathology are closely associated with inflammation, proinflammatory factors, including TNF-α and IL-1β, and anti-inflammatory factors, including IL-4 and IL-10, were detected via ELISA kits to evaluate the therapeutic effects of Exos-Ber/Pal on neuroinflammation. The results suggested that compared with the AD model group and the Ber/Pal-free drug treatment group, the Exos-Ber/Pal treatment group exhibited pronounced amelioration of neuroinflammation by reducing the levels of proinflammatory factors, including TNF-α and IL-1β, and increasing the levels of anti-inflammatory factors, including IL-4 and IL-10 (Figure 8H–K). In summary, these results suggested the excellent and significantly elevated AD symptom-improving effects of the microglia-derived Exos delivery method compared with Ber/Pal free drug treatment in AD model mice.

Discussion

AD is a neurodegenerative disease characterized by Aβ plaque deposition, Tau phosphorylation, and neurodegeneration.[18] Neuroinflammation and microglia are research hotspots of neurodegenerative diseases.[19,20] At present, there are no completely effective drugs that have been approved for clinical treatment because of the multifactorial characterization of AD.[21] Current mainstream therapeutic drugs for AD are cholinesterase inhibitors, including donepezil, galantamine, and NMDAR antagonists encompassing rivastigmine and memantine.[22] However, these drugs can only alleviate the symptoms of AD and have serious adverse drug reactions.[23] Additionally, despite FDA approval of the monoclonal antibody

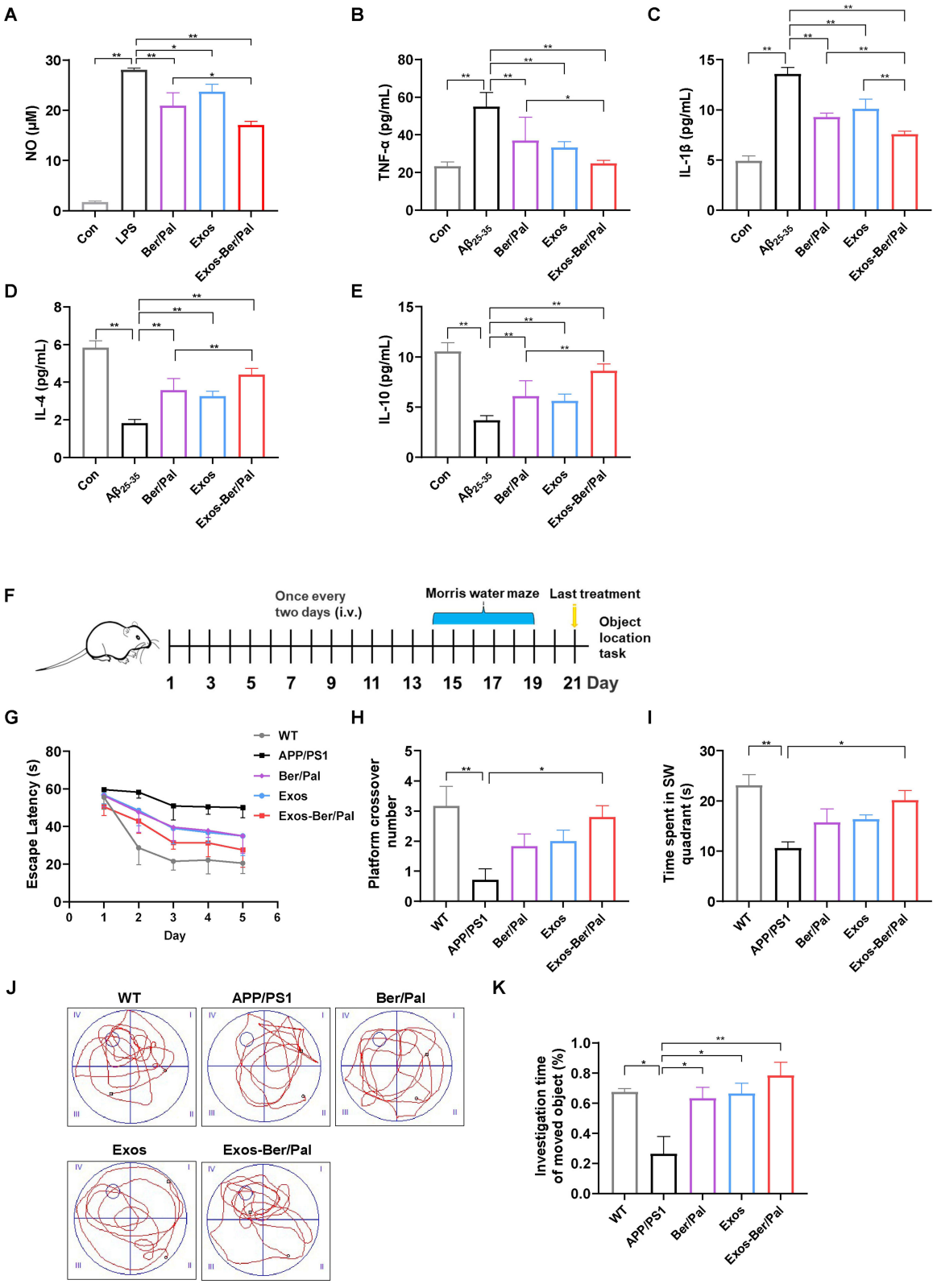

Figure 6 Effect of Exos-Ber/Pal on neuroinflammation in vitro and behaviour in APP/PS1 mice. (**A**) The NO concentration in LPS-stimulated (250 ng/mL) microglia was detected with the Griess method. (**B**–**E**) Inflammatory cytokine detection of TNF-α, IL-1β, IL-4 and IL-10. Inflammatory cytokines in microglia stimulated by $A\beta_{25-35}$ (20 μM) after coincubation with Ber/Pal, Exos and Exos-Ber/Pal for 24 h. The microglia were stimulated with LPS/$A\beta_{25-35}$ for 1 h in advance. The concentration of Ber/Pal was 0.3 μM. (**F**) Schematic illustration of the experiment. (**G**) The escape latency time, (**H**) platform crossing times, and (**I**) target quadrant occupancy in the MWM. (**J**) Representative motion trajectories in the MWM. i, the first quadrant of MWM; ii, the second quadrant of MWM; iii, the third quadrants of MWM; iv, the fourth quadrants of MWM. (**K**) OLT performance of mice administered different formulations. WT indicates wild-type control mice without any gene intervention. APP/PS1 indicates the AD model mice. The Ber/Pal injection dosage was 1.22/1.52 mg/kg. (**A**), n = 3; (**B**–**E**), n = 6; (**F**–**K**), n = 8. *p < 0.05, **p < 0.01.

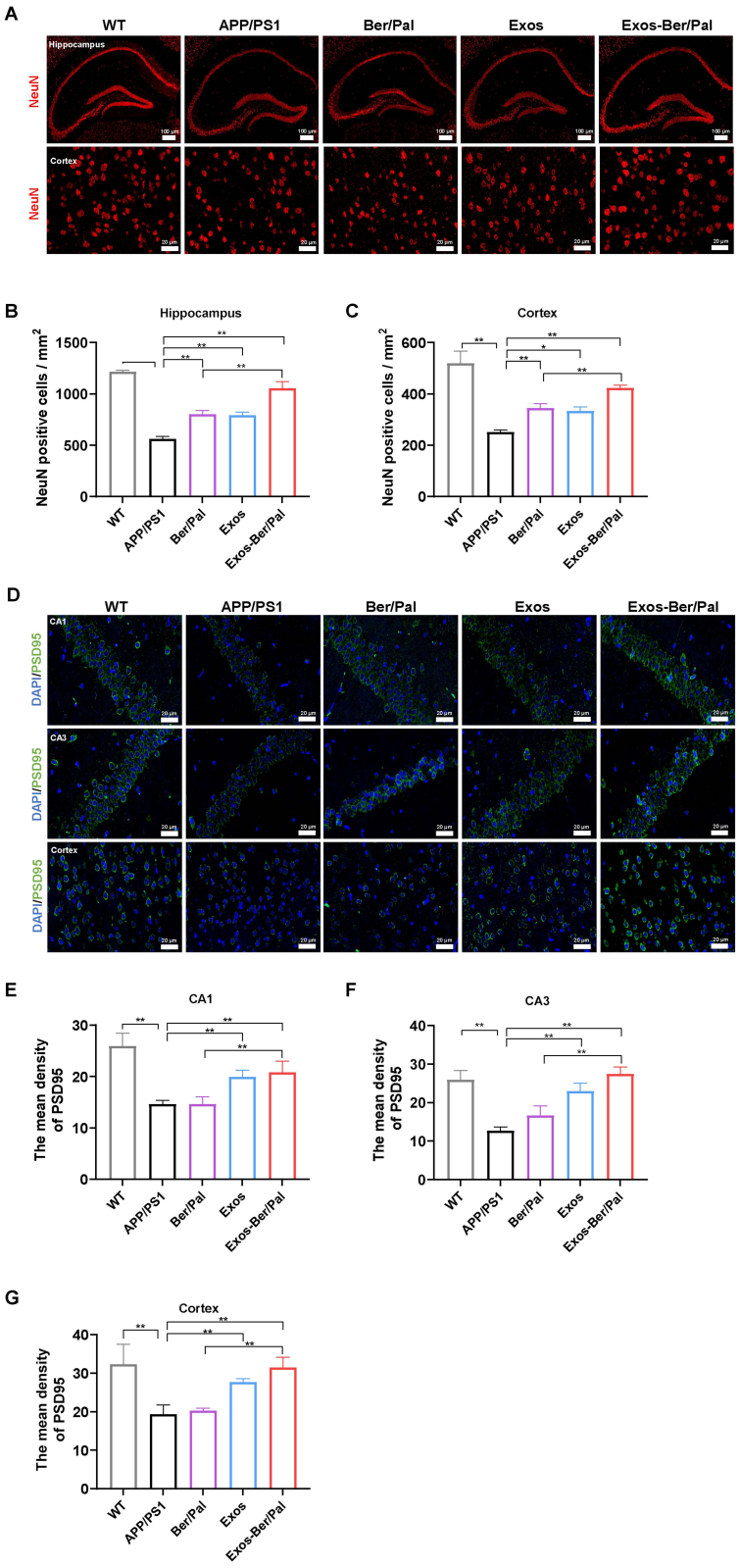

Figure 7 Effect of Exos-Ber/Pal on neuronal recovery in APP/PS1 mice. (**A**) Immunofluorescence staining of NeuN-positive cells and (**B** and **C**) NeuN-positive cell counting in the hippocampus and cortex. (**D**) Immunofluorescence observation and (**E**–**G**) semiquantitative data of PSD95 in the CA1, CA3 and cortex. WT indicates wild-type control mice without any gene intervention. APP/PS1 indicates the AD model mice. The Ber/Pal injection dosage was 1.22/1.52 mg/kg. The scale bar for (**A**) is 100 μm (hippocampus) and 20 μm (cortex). The scale bar for (**D**) is 20 μm. n = 3. *p < 0.05, **p < 0.01.

https://doi.org/10.2147/DDDT.S417465

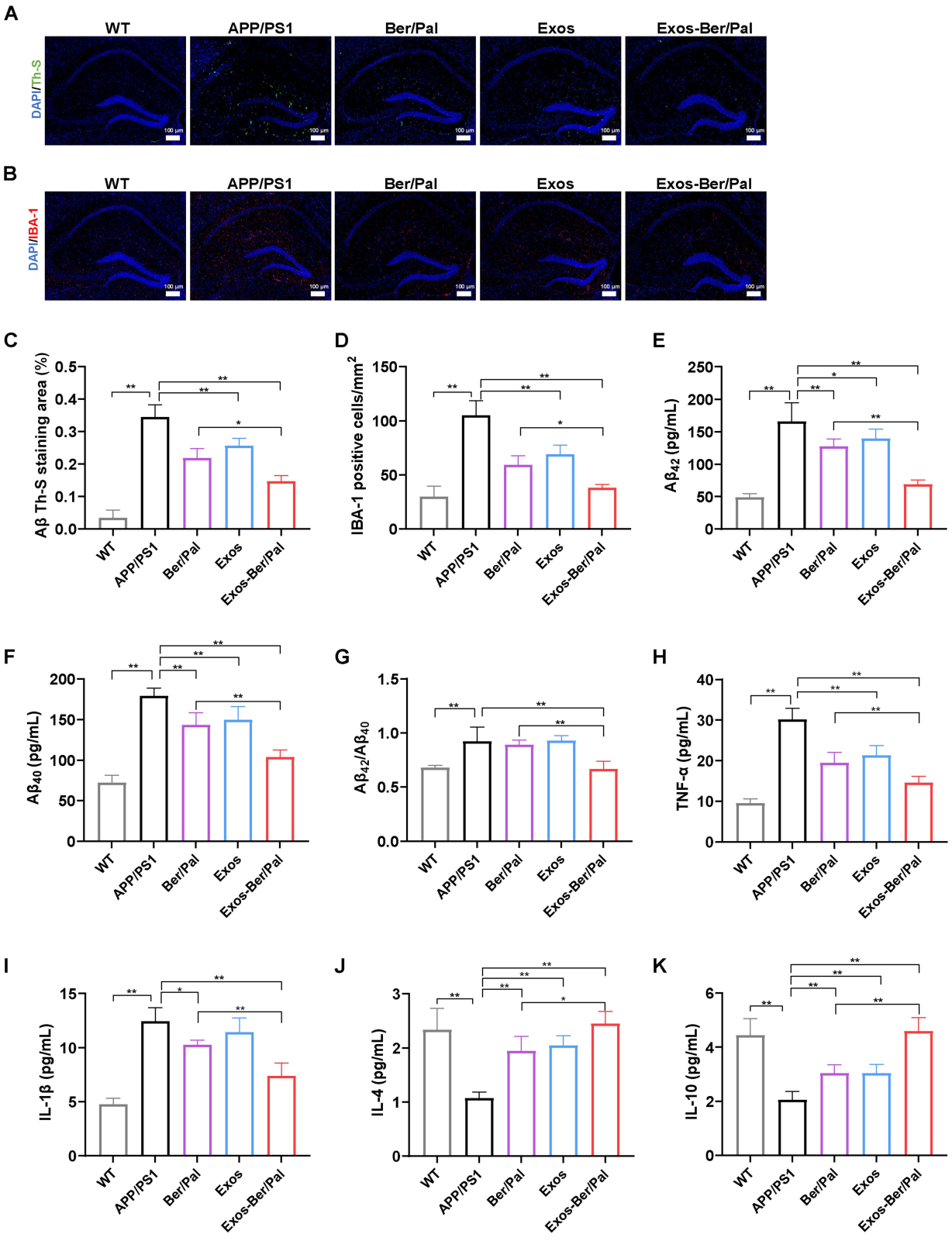

Figure 8 Effect of Exos-Ber/Pal on plaque inhibition, microglial activation and inflammation in APP/PS1 mice. Immunofluorescence staining observation of (**A**) Th-S (Aβ) and (**B**) IBA-1 in the hippocampus. Quantitative analysis of (**C**) Aβ and (**D**) IBA-1. (**E**–**G**) Concentration determination of $A\beta_{42}$ and $A\beta_{40}$ and the ratio of $A\beta_{42}/A\beta_{40}$ in the hippocampus by ELISA. (**H**–**K**) Inflammatory cytokine detection of TNF-α, IL-1β, IL-4 and IL-10 in the hippocampus. WT indicates wild-type control mice without any gene intervention. APP/PS1 indicates the AD model mice. The Ber/Pal injection dosage was 1.22/1.52 mg/kg. The scale bar is 100 μm. (**A**–**D**), n = 3. (**E**–**K**), n = 5. *p < 0.05, **p < 0.01.

aducanumab against the Aβ peptide, its effectiveness in improving cognitive function remains widely debated.[24] Accordingly, there is an urgent need to find new effective drugs for AD clinical treatment.

Considering the multifactorial characterization of AD, multitarget and multi-pathway combination methods are gradually emerging as potential therapies.[25] Accordingly, synergistic drug combinations have shown increasing significance in clinical therapy due to their promise in providing superior therapeutic benefits to the current drug combination therapy used in clinical practice.[26] Phytoconstituents are a rich source of lead molecules for drug discovery and development with the characterization of multitargets, regulating multiple pathogenic pathways, low toxicity and rare adverse effects.[27] However, only a few drugs have been approved for clinical application due to their low bioavailability, poor solubility, and difficulty in passing through the BBB.[28] Studies have shown that nasal sprays, mixed micelles, and nanocarriers can improve bioavailability and crossing of the BBB in neurodegenerative diseases.[29–31] As a natural delivery carrier, Exos have stronger biocompatibility than other nanocarriers to prevent clearance by the immune system, and their natural targeting ability enhances their permeability to the brain due to their biogenic origin.[32,33] NIH-registered clinical experiments related to Exos include the neuroprotection of Exos in infants, diagnosis of diseases such as cerebral haemorrhage and stroke, and treatment of neurodegenerative diseases such as depression, anxiety, and dementia.[34,35] Herein, Exos derived from microglia were used as carriers of Ber/Pal, which showed excellent anti-inflammatory effects both in vitro and in vivo; enhanced drug accumulation in the hippocampus, cortex, and striatum; and improved cognitive impairment and nerve injury in the APP/PS1 AD model by accelerating Aβ elimination and anti-inflammatory cytokine secretion.

For the present study, our experiment mainly focused on the therapeutic efficacy of Ber, Pal and the Ber/Pal combined treatment method in vitro and in vivo. As reported, the abnormal metabolism of sphingolipids plays an essential role in the pathogenesis of AD.[36] The ratio of S1P/Cer determines cell proliferation and survival.[37] In AD, the level of Cer is significantly increased, which has toxic effects on neurons and promotes the secretion of inflammatory cytokines.[38] Additionally, Cer also promotes Aβ formation by stabilizing β-site APP cleaving enzyme 1 activity.[39] HLJDD has been utilized to treat dementia and improve learning and memory impairments.[40] Our previous study showed that HLJDD treated AD by affecting sphingolipid metabolism.[41] HLJDD regulated the decrease in S1P levels and the increase in Cer levels in microglia caused by $A\beta_{25\text{-}35}$ stimulation, which was also reflected in the treatment of APP/PS1 mice. As natural phytoconstituents, Ber and Pal exert effective anti-inflammatory and neuroprotective effects in neurodegenerative diseases. In the treatment of neuroinflammation, Ber and Pal intervene through multiple targets. Studies have shown that Ber may inhibit the activation of NF-κB by blocking the PI3K/PKB and MAPK signalling pathways while activating the AMPK pathway to inhibit the inflammatory response of microglia, which is consistent with our inflammatory factors as well as bioinformatics results.[42]

Nevertheless, although our study suggested that Exos-Ber/Pal therapy could promote the targeting and permeation of drugs into the brain, there are some limitations in our study. For example, the low yield of cell-derived Exos and the long preparation time limit their application in clinical treatment. During the extraction process, every 2.13×10^8 cells produced 1 mg of Exos. The amount of Exos used in animal experiments was approximately 70.4 mg, which came from 5.63×10^{10} cells. Therefore, it is necessary to explore methods to improve Exo production and reduce its costs. Notably, some studies have shown that the yield of Exos can be significantly increased dozens of times through low-level electrical treatment (0.34 mA/cm2) and production boosters, providing a promising Exos preparation method.[43,44]

Additionally, our distribution results of Exos-Ber/Pal suggested that a small amount of Exos-Ber/Pal could permeate into the heart and kidney (Figure S7), suggesting the limitation of the lack of organic targeting. Accordingly, it is necessary to modify and decorate Exos to promote their specificity in brain targeting, such as through genetic engineering, bioengineering, and physical engineering.[45] The system-specific rabies virus glycoprotein peptide and angiopep-2 are promising ligands to target peptides to the nervous system.[46] In the future, our research will focus more on optimizing the Exos extraction method, modification and transformation to improve the precise targeting of Exos and on improving their roles in the treatment and recovery of neurodegenerative diseases.

Conclusion

Our results initially explored the therapeutic effects of Ber and Pal on AD, which include protecting neurons and alleviating synaptic damage, ameliorating Aβ pathological symptoms by promoting phagocytosis of Aβ plaques by microglia and inhibiting neuroinflammation. Additionally, the Ber and Pal combined therapy exhibits better and more

comprehensive therapeutic effects than single-drug treatment but relatively limited improvement in the therapeutic effects, confirming the feasibility of Ber and Pal combined therapy in AD treatment. However, our data also suggested defects in BBB permeability via ADMET computational prediction, and to improve the BBB permeation and targeting ability of Ber/Pal combined treatment, we utilized microglia-derived Exos as drug carriers and verified that the microglia-derived Exos delivery method could enhance the therapeutic effects of Ber/Pal free drug treatment.

Abbreviations

AD, Alzheimer's disease; Aβ, β-amyloid; Ber, berberine; Pal, palmatine; BBB, blood–brain barrier; CNS, central nervous system; NO, nitric oxide; Jat, jatrorrhizine; Brb, berberrubine; Wog, wogonin; Bai, baicalin; OA, oroxylin A; GB, gardenin B; Gen, geniposide; Exos, exosomes; NTA, nanoparticle tracking analysis; TEM, transmission electron microscope; WB, Western blotting; MWM, Morris water maze; OLT, object location task; WT, wild type; IF, immunofluorescence.

Institutional Review Board Statement

The animal study protocol was approved by the Experimental Animal Care and Use Committee of Nanjing University of Traditional Chinese Medicine and was approved on 19 December 2022 (project proposal number 202212A003). The study was performed following recommendations provided by the Guide for the Care and Use of Laboratory Animals of the National Institutes of Health (NIH Publication No. 80–23; revised 1978).

Data Sharing Statement

Data will be made available on request. The original data in this study can be obtained from the corresponding author (Qichun Zhang).

Funding

This study was financially supported by the National Natural Science Foundation of China (Project Nos. 81873027 and 81573635), the Qing-Lan Project of Jiangsu Province, the Open Project Program of Jiangsu Key Laboratory for Pharmacology and Safety Evaluation of Chinese Materia Medica (No. JKLPSE201820), the Project Funded by the Priority Academic Program Development of Jiangsu Higher Education Institutions (PAPD), the Project of the Innovation Research Team of Nanjing University of Chinese Medicine, and the Project Funded by the Six Talent Project in Jiangsu Province.

Disclosure

Xin Zhao and Pingyuan Ge are co-first authors for this study. The authors declare no conflicts of interest in this work.

References

1. Webers A, Heneka MT, Gleeson PA. The role of innate immune responses and neuroinflammation in amyloid accumulation and progression of Alzheimer's disease. *Immunol Cell Biol*. 2020;98(1):28–41. doi:10.1111/imcb.12301
2. Vay SU, Flitsch LJ, Rabenstein M, et al. The plasticity of primary microglia and their multifaceted effects on endogenous neural stem cells in vitro and in vivo. *J Neuroinflamm*. 2018;15(1):226. doi:10.1186/s12974-018-1261-y
3. Ismail R, Parbo P, Madsen LS, et al. The relationships between neuroinflammation, beta-amyloid and tau deposition in Alzheimer's disease: a longitudinal PET study. *J Neuroinflamm*. 2020;17(1):151. doi:10.1186/s12974-020-01820-6
4. Roddan R, Subrizi F, Broomfield J, et al. Chemoenzymatic cascades toward methylated tetrahydroprotoberberine and protoberberine alkaloids. *Org Lett*. 2021;23(16):6342–6347. doi:10.1021/acs.orglett.1c02110
5. Tao C, S-q H, Chen J, et al. Highly efficient synthesis and monoamine oxidase B inhibitory profile of demethyleneberberine, columbamine and palmatine. *Neurochem Int*. 2020;139:104807. doi:10.1016/j.neuint.2020.104807
6. Wang S, Lee DY-W, Shang Y, et al. The bioactive alkaloids identified from cortex phellodendri ameliorate benign prostatic hyperplasia via LOX-5/COX-2 pathways. *Phytomedicine*. 2021;93:153813. doi:10.1016/j.phymed.2021.153813
7. Akbar M, Shabbir A, Rehman K, et al. Neuroprotective potential of berberine in modulating Alzheimer's disease via multiple signaling pathways. *J Food Biochem*. 2021;45(10):e13936. doi:10.1111/jfbc.13936
8. Kiris I, Kukula-Koch W, Karayel-Basar M, et al. Proteomic alterations in the cerebellum and hippocampus in an Alzheimer's disease mouse model: alleviating effect of palmatine. *Biomed Pharmacother*. 2023;158:114111. doi:10.1016/j.biopha.2022.114111
9. Mak S, Luk WWK, Cui W, et al. Synergistic inhibition on acetylcholinesterase by the combination of berberine and palmatine originally isolated from Chinese medicinal herbs. *J Mol Neurosci*. 2014;53(3):511–516. doi:10.1007/s12031-014-0288-5

10. Han L, Jiang C. Evolution of blood-brain barrier in brain diseases and related systemic nanoscale brain-targeting drug delivery strategies. *Acta Pharmaceutica Sinica B*. 2021;11(8):2306–2325. doi:10.1016/j.apsb.2020.11.023
11. Liao J, Fan L, Li Y, et al. Recent advances in biomimetic nanodelivery systems: new brain-targeting strategies. *J Control Release*. 2023;358:439–464. doi:10.1016/j.jconrel.2023.05.009
12. Arshaghi TE, Clifford J, Davies S, et al. Mesenchymal stem cell exosome characterisation and high-throughput quantification by fluorescence polarisation spectroscopy. *Cytotherapy*. 2020;22(5):S48. doi:10.1016/j.jcyt.2020.03.057
13. Zhu S, Huang H, Liu D, et al. Augmented cellular uptake and homologous targeting of exosome-based drug loaded IOL for posterior capsular opacification prevention and biosafety improvement. *Bioact Mater*. 2022;15:469–481. doi:10.1016/j.bioactmat.2022.02.019
14. Tang B, Zeng W, Song LL, et al. Extracellular vesicle delivery of neferine for the attenuation of neurodegenerative disease proteins and motor deficit in an Alzheimer disease mouse model. *Pharmaceuticals*. 2022;15(1):83. doi:10.3390/ph15010083
15. Qi YY, Heng X, Yao ZY, et al. Involvement of Huanglian Jiedu decoction on microglia with abnormal sphingolipid metabolism in Alzheimer's disease. *Drug Des Dev Ther*. 2022;16:931–950. doi:10.2147/DDDT.S357061
16. Vorhees CV, Williams MT. Morris water maze: procedures for assessing spatial and related forms of learning and memory. *Nat Protoc*. 2006;1(2):848–858. doi:10.1038/nprot.2006.116
17. Bevins RA, Besheer J. Object recognition in rats and mice: a one-trial non-matching-to-sample learning task to study 'recognition memory'. *Nat Protoc*. 2006;1(3):1306–1311. doi:10.1038/nprot.2006.205
18. Spina S, La Joie R, Petersen C, et al. Comorbid neuropathological diagnoses in early versus late-onset Alzheimer's disease. *Brain*. 2021;144(7):2186–2198. doi:10.1093/brain/awab099
19. Feldman RA. Microglia orchestrate neuroinflammation. *eLife*. 2022;11:e81890. doi:10.7554/eLife.81890
20. Ottoy J, Bezgin G, Savard M, et al. Microglia activation predicts tau positivity beyond Aβ in Alzheimer's disease. *Alzheimers Dement*. 2021;17(S1):e054667. doi:10.1002/alz.053125
21. Hausner L, Frölich L. Medikamentöse therapie der Alzheimer-Demenz mit antidementiva [Antidementia drug therapy of Alzheimer's Dementia: status 2018 and outlook]. *Dtsch Med Wochenschr*. 2019;144(03):156–160. German. doi:10.1055/a-0658-6720
22. Bachurin SO, Bovina EV, Ustyugov AA. Drugs in clinical trials for Alzheimer's disease: the major trends. *Med Res Rev*. 2017;37(5):1186–1225. doi:10.1002/med.21434
23. Hung S-Y, Fu W-M. Drug candidates in clinical trials for Alzheimer's disease. *J Biomed Sci*. 2017;24(1):47. doi:10.1186/s12929-017-0355-7
24. Iqbal K. Thinking beyond the aducanumab controversy. *Ann Neurol*. 2021;90(6):1003–1004. doi:10.1002/ana.26252
25. Haghighijoo Z, Akrami S, Saeedi M, et al. N-Cyclohexylimidazo[1,2-a]pyridine derivatives as multi-target-directed ligands for treatment of Alzheimer's disease. *Bioorg Chem*. 2020;103:104146. doi:10.1016/j.bioorg.2020.104146
26. Weinstein JD. A unique and promising combination of medications for the treatment of Alzheimer's disease. *Med Hypotheses*. 2017;109:53–55. doi:10.1016/j.mehy.2017.09.021
27. Ahmad A, Tandon S, Xuan TD, et al. A review on phytoconstituents and biological activities of cuscuta species. *Biomed Pharmacother*. 2017;92:772–795. doi:10.1016/j.biopha.2017.05.124
28. Haque A, Brazeau D, Amin AR. Perspectives on natural compounds in chemoprevention and treatment of cancer: an update with new promising compounds. *Eur J Cancer*. 2021;149:165–183. doi:10.1016/j.ejca.2021.03.009
29. Liu N, Li Y, Liu L, et al. Administration of silver nasal spray leads to nanoparticle accumulation in rat brain tissues. *Environ Sci Technol*. 2022;56(1):403–413. doi:10.1021/acs.est.1c02532
30. Katekar R, Thombre G, Riyazuddin M, et al. Pharmacokinetics and brain targeting of trans-resveratrol loaded mixed micelles in rats following intravenous administration. *Pharm Dev Technol*. 2020;25(3):300–307. doi:10.1080/10837450.2019.1680690
31. Comoglu T, Arisoy S, Akkus BZ. Nanocarriers for effective brain drug delivery. *Curr Top Med Chem*. 2017;17(13):1490–1506. doi:10.2174/1568026616666161222101355
32. Lin Y, Lu Y, Li X. Biological characteristics of exosomes and genetically engineered exosomes for the targeted delivery of therapeutic agents. *J Drug Target*. 2020;28(2):129–141. doi:10.1080/1061186X.2019.1641508
33. Pi Y-N, Xia B-R, Jin M-Z, et al. Exosomes: powerful weapon for cancer nano-immunoengineering. *Biochem Pharmacol*. 2021;186:114487. doi:10.1016/j.bcp.2021.114487
34. Happel C, Peñalber-Johnstone C, Tagle DA. Pivoting novel exosome-based technologies for the detection of SARS-CoV-2. *Viruses*. 2022;14(5):1083. doi:10.3390/v14051083
35. Salarpour S, Barani M, Pardakhty A, et al. The application of exosomes and exosome-nanoparticle in treating brain disorders. *J Mol Liq*. 2022;350:118549. doi:10.1016/j.molliq.2022.118549
36. Crivelli SM, Giovagnoni C, Visseren L, et al. Sphingolipids in Alzheimer's disease, how can we target them? *Adv Drug Deliv Rev*. 2020;159:214–231. doi:10.1016/j.addr.2019.12.003
37. Puig N, Estruch M, Jin L, et al. The role of distinctive sphingolipids in the inflammatory and apoptotic effects of electronegative LDL on monocytes. *Biomolecules*. 2019;9(8):300. doi:10.3390/biom9080300
38. Torretta E, Arosio B, Barbacini P, et al. Particular CSF sphingolipid patterns identify iNPH and AD patients. *Sci Rep*. 2018;8(1):13639. doi:10.1038/s41598-018-31756-0
39. Brodowicz J, Przegaliński E, Müller CP, et al. Ceramide and its related neurochemical networks as targets for some brain disorder therapies. *Neurotox Res*. 2018;33(2):474–484. doi:10.1007/s12640-017-9798-6
40. Liu Y, Du T, Zhang W, et al. Modified Huang-Lian-Jie-Du decoction ameliorates Aβ synaptotoxicity in a murine model of Alzheimer's disease. *Oxid Med Cell Longev*. 2019;2019:8340192. doi:10.1155/2019/8340192
41. Zhu B, Cao H, Sun L, et al. Metabolomics-based mechanisms exploration of Huang-Lian Jie-Du decoction on cerebral ischemia via UPLC-Q-TOF/MS analysis on rat serum. *J Ethnopharmacol*. 2018;216:147–156. doi:10.1016/j.jep.2018.01.015
42. Chen J, Huang Y, Bian X, et al. Berberine ameliorates inflammation in acute lung injury via NF-κB/Nlrp3 signaling pathway. *Oxid Med Cell Longev*. 2022;9:851255.
43. Zhao Z, Qu L, Shuang T, et al. Low-intensity ultrasound radiation increases exosome yield for efficient drug delivery. *J Drug Deliv Sci Technol*. 2020;57:101713. doi:10.1016/j.jddst.2020.101713

44. Gao M, Cai J, Zitkovsky HS, et al. Comparison of yield, purity, and functional properties of large-volume exosome isolation using ultrafiltration and polymer-based precipitation. *Plast Reconstr Surg*. 2022;149(3):638–649. doi:10.1097/PRS.0000000000008830
45. Li M, Li S, Du C, et al. Exosomes from different cells: characteristics, modifications, and therapeutic applications. *Eur J Med Chem*. 2020;207:112784. doi:10.1016/j.ejmech.2020.112784
46. Zhu Z, Zhai Y, Hao Y, et al. Specific anti-glioma targeted-delivery strategy of engineered small extracellular vesicles dual-functionalised by Angiopep-2 and TAT peptides. *J Extracell Vesicles*. 2022;11(8):e12255. doi:10.1002/jev2.12255